Observations of CO_2 Corrosion Induced Carbonate Scale Formation and Inhibition on Mild Steel

Wei Li*, Zhaoyi Dai*, Xin Wang, Saebom Ko, Samiridhdi Paudyal, Xuanzhu Yao, Cianna Leschied, Yu-Yi Shen, Daniel Pimentel, Amy T. Kan, Mason B. Tomson

Department of Civil and Environmental Engineering, Rice University, Houston, Texas 77005, United States

*Corresponding authors; emails: WL234208@gmail.com (W. Li); dzy616@gmail.com (Z. Dai).

Keywords: Mild steel; CO_2 corrosion; calcite; ankerite; scale inhibitor.

Summary

Aqueous CO_2-containing environment is ubiquitous in oil and gas production. Carbonate scales (e.g., calcite) tend to form in such an environment. Meanwhile, the CO_2 corrosion of mild steel infrastructure may result in corrosion-induced scales including $FeCO_3$ (siderite). Previously, siderite was generally treated as a corrosion problem rather than a scale problem. However, the relationship between the corrosion-induced scale and other metal carbonate scales on the steel surface is unclear. For example, how does siderite influence calcite deposition on the mild steel? In this study, the mild steel corrosion and mineral carbonate scaling behaviors were investigated simultaneously in the presence of various cations such as Ca^{2+} and Mg^{2+}. We observed a two-layer scale structure on the mild steel surface under simulated oilfield conditions. The inner layer is an iron-containing carbonate scale such as ankerite or siderite, while the outer layer is calcite. In

addition, calcite deposition at very low saturation index was observed when the inner layer was present. Furthermore, a common scale inhibitor (DTPMP) can effectively mitigate calcite, siderite and ankerite formation on the steel surface, but meanwhile, aggravate the steel corrosion due to the absence of protective scale layers.

Introduction

Sweet (CO_2 containing) conditions are frequently encountered in the upstream oil and gas operations as both CO_2 and water are natural constituents in petroleum reservoirs (Cavenati et al. 2006, Danesh 1998). Almost all oil production infrastructure, such as production tubing, flowlines, storage facilities, and transportation pipelines, etc., is made of low-carbon (mild) steels due to their versatile mechanical properties and relatively low cost. However, when this CO_2-dissolved formation water traversing production infrastructure, it often creates two engineering problems: internal corrosion and mineral scale deposition.

The dissolved CO_2 in the water forms carbonic acid (H_2CO_3), H^+, HCO_3^- and CO_3^{2-} through hydration and dissociation reactions (Li et al. 2014). Mild steel tends to be corroded and releases ferrous ions in aqueous CO_2 environment. The general CO_2 corrosion mechanisms have been extensively researched and well understood (Kahyarian et al. 2017, Nesic 2012). A common CO_2 corrosion byproduct, iron carbonate ($FeCO_3$), may form, propagate on internal steel surface and protect the steel from further corrosion (Greenberg and Tomson 1992, Johnson and Tomson 1991, Joshi et al. 2018, Li et al. 2014, 2015). Simultaneously, the mineral ions such as Ca^{2+} and Mg^{2+} in the formation water (Blondes et al.2018, Kelland 2014) can react with the carbonate ion and precipitate on the steel surface in the form of carbonate scales (e.g., $CaCO_3$ and $MgCO_3$) under

specific operating conditions (Kelland 2014, Amjad and Demadis 2015). Furthermore, in addition to the single cation carbonate formation (e.g., $FeCO_3$, $CaCO_3$ and $MgCO_3$), the multi-cation carbonate scale can form (e.g., Dolomite ($CaMg(CO_3)_2$) or Ankerite ($Ca(Fe,Mg)(CO_3)_2$)) (Railsback 1999). Continuous deposition of these carbonate minerals can reduce production and compromise operation safety.

Probably due to the fact that $FeCO_3$ scale is mainly observed as a corrosion byproduct of mild steel, it is often studied as a corrosion problem instead of a scale problem. In addition, conventional corrosion and scaling studies have very different testing timescales. The former one is often within the timescale of days or weeks to understand the environmental impacts on the steel surface, while the later one is commonly on a timescale of seconds or hours with a focus on scale formation kinetics in the bulk water chemistry. As corrosion and mineral scale deposition both occur on the mild steel surface simultaneously, dealing with them as a whole provides a more accurate understanding of what is happening during oil and gas production. However, studies using this approach are scarce in the open literature. Few corrosion studies of such showed that the presence of Mg^{2+} and Ca^{2+} in the bulk solution changes the protectiveness of $FeCO_3$ layer and forms co-precipitation such as mixed iron-calcium carbonate ($Fe_xCa_{1-x}CO_3$), which were summarized in a recent review (Barker et al. 2018). Many of those studies utilize testing systems like ambient pressure glass cell (Joshi et al. 2018, Mansoori et al. 2019), high-pressure autoclave (Ding et al. 2009), or continuous stirred tank reactor (Alsaiari et al. 2010, Ieamsupapong et al. 2017). These systems are either a closed system or an open system with some reactor characteristics in terms of mass exchange, which also have unique geometries and flow behavior. None of these systems closely resembles an oilfield production scenario with corrosion and scaling processes, in which brines continuously travel through and react with the internal surface of a mild steel conduit

(tubing, pipeline, piping, etc.) (Javaherdashti et al. 2013, Li et al. 2016). Therefore, those laboratory testing results may be not directly translatable to oilfield conditions. Instead, a once-through flow cell (plug flow reactor) (Fogler 2016) can better simulate realistic oilfield conditions, and it has been used in studies for many common oilfield scales, such as barium sulfate, calcium carbonate, etc. (Bukuaghangin et al. 2016, Harouaka et al. 2018, Lu et al. 2020).

In this study, a once-through flow cell apparatus was utilized to study the mild steel tubing corrosion and scaling behavior simultaneously in the presence of multiple metal cations. The corrosion product chemical composition, structure, and its interaction with bulk solution for further scale deposition were investigated. Furthermore, the efficacy of conventional scaling inhibition methods on the mild steel corrosion induced scale formation was studied. The results showed that a new corrosion-induced scale, ankerite, was observed in a wide range of conditions. The ankerite scale further promoted bulk calcite deposition. In addition, DTPMP was found to be effective for corrosion-induced scale inhibition, including ankerite.

Experimental Procedures

Methods

A once-through flow cell was used for the experiments, as depicted in **Fig. 1**. In each test, two stock solutions were prepared in a 0.5 or 1.0 m (molality) NaCl background solution. Metal ions of interest such as Ca^{2+} and Mg^{2+} were added into the cation stock solution in the form of reagent grade $CaCl_2 \cdot 2H_2O$ and $MgCl_2 \cdot 6H_2O$ (Sigma Aldrich^{TM}), respectively. $NaHCO_3$ was added into the anion stock solution to reach a targeted alkalinity value and for the pH adjustment of the final reacting solutions. For some scale inhibition tests, scale inhibitors were added into the anion stock

solution as well. The stock solutions were continuously purged with CO_2 gas (100% (v/v) or 10% balanced with argon) during the whole experiments at ambient conditions. Two oxygen traps were used in tandem after the gas cylinder outlet to reduce oxygen concentration below 1 ppb (part per billion, 10^{-9}). All connection lines in the system are made of either low oxygen permeable polyether ether ketone (PEEK) or AISI (American Iron and Steel Institute) 316 stainless steel tubing. No additional Fe^{2+} source was added into the stock solutions. As a result, all Fe^{2+} in the test was from the corrosion of the mild steel specimen inside the reactor to mimic oilfield production conditions. Hydrolamine hydrochloride was also added to the stock solutions to prevent oxidation of Fe^{2+} inside the reactor (Li et al. 2018). The chemical concentrations and saturation index of calcite in the stock solutions were calculated using the ScaleSoftPitzer^{TM} (SSP) software (Kan et al. 2018) to achieve a desired water chemistry inside the reactor at testing conditions. After at least 3 hours of gas purging into the entire apparatus, the stock solutions were injected to a flow tee at a constant flow rate using two syringe pumps. The mixed solution then traveled through the mild steel tube specimens inside a glass tube reactor (6.80 mm inner diameter) immersed in a water bath at a constant temperature.

ASTM (American Society for Testing and Materials) A179 mild steel tubing, AISI 1018 mild steel tubing, and AISI 316 stainless steel tubing specimens (nominal dimensions: 6.35 mm outer diameter, 1.27 mm wall thickness, 25.4 mm long) were used. Because A179 and 1018 mild steel specimens showed similar preliminary experimental results in this study, they were generally denoted mild steel specimens hereafter without further differentiation. All specimens were pre-cut into two equal halves along the tubing axial direction by a low speed cutting machine (Buehler IsoMet^{TM}). The specimen external surfaces were coated with a corrosion-resistance spray paint (Rust-Oleum^{TM}); and the internal surfaces were sequentially polished with 200, 400, and 600 grit

SiC sand papers. The pre-treated two halves were then joined together as a whole tubing piece by wrapping adhesive tape around the external surfaces. The tubing specimens were then inserted into the glass tube reactor. As a seal was made between the external surface of the specimens and the glass tube internal wall, fluid flow traverses the internal wall of steel tubing specimens during a test.

A back pressure regulator (BPR) was used downstream of the reactor to maintain a sufficient pressure that can suppress the water vapor bubble generation and CO_2 degassing at elevated testing temperatures. The depressurized effluent after BPR was collected for water chemistry monitoring on the concentrations of ferrous ion, alkalinity and calcium ion by colorimetric methods (i.e., Hach™ total iron FerroVer method, Hanna™ saltwater aquarium alkalinity and calcium colorimeters).

After each test, the steel specimens were taken out and immediately rinsed with deionized water to remove any soluble salts on the surface. The specimens were then immersed into isopropanol and cleaned by ultrasonication to remove loose corrosion or scaling product. After cleaning, the specimens were stored in a desiccator for further surface analysis. A scanning electron microscopy – Energy dispersive spectroscopy (SEM-EDS) system (FEI™) was used to obtain the surface morphology and chemical compositional information of the specimens. An X-ray diffraction system (Rigaku™) with a Cu target was utilized to identify mineral phases formed on the steel surface. The scan range was from 20 to 80° with a scan rate of 5°/min. The measured XRD patterns were then compared to the ICDD-PDF 4 (International Centre for Diffraction Data - Powder Diffraction File) database for phase identification. The reference intensity ratio (RIR) method was also used for semi-quantitative phase compositional analysis. RIR details can be referred to elsewhere (Hubbard and Snyder, 1988). Cross sectional analysis of the tube specimen (along the

tube radial direction) was performed to analyze the structure of the formed surface scale layers when necessary. To prepare a cross sectional sample, a castable epoxy was first poured onto the half-piece tube specimen internal surface to preserve the scale layers. Once the epoxy was cured, the specimen was cut through the tube radial direction using a low speed cutting machine. The cut surface was then polished sequentially using from 200 to 2000 grit sand papers. After that, the sample was coated with gold using a sputter if necessary. Finally, the sample cut surface was analyzed by a SEM.

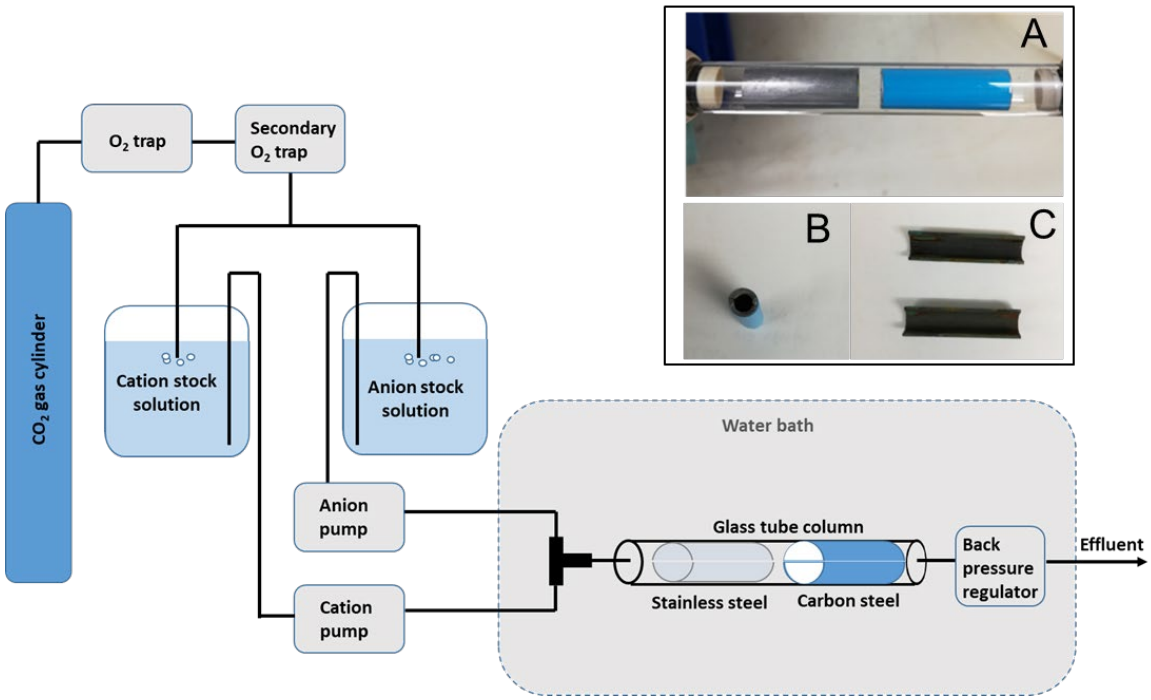

Fig. 1—Schematic of the once-through flow cell apparatus. Inset Picture A: stainless steel and mild steel specimens inside the glass tube column; Picture B: mild steel specimen seen from axial direction; Picture C: mild steel specimen halves after testing with corrosion seen from top.

Experimental Conditions

We analyzed the USGS (United States Geological Survey) produced water database (Blondes 2018) in order to select proper concentrations of some key ions interested. As shown in **Table 1**, ion concentrations vary with wide ranges in the produced waters. Nevertheless, Ca^{2+} and Mg^{2+} are normally present in the water with a significant level. An important driving force for the divalent cation carbonate formation is solution supersaturation, and is often described as saturation index (SI), as given by:

$$SI = \log_{10}\left(\frac{a_{Me^{2+}} a_{CO_3^{2-}}}{K_{sp,\,MeCO_3}}\right) \quad (1)$$

where *SI* is saturation index, $a_{Me^{2+}}$ is the divalent cation (Fe^{2+}, Mg^{2+}, or Mg^{2+}) activity in solution, $a_{CO_3^{2-}}$ is the carbonate anion activity in solution, $K_{sp,\,MeCO_3}$ is the solubility product constant of the respective metal carbonate.

We subsequently selected two representative water chemistry scenarios for testing that are often encountered in the oilfield, as shown in **Table 2**. The testing flow rates varied in a limited range from 30 mL/h to 80 mL/h in this study, as the flow effect was not the focus.

Table 1—Statistics of key ion concentrations from the USGS produced water database (Blondes 2018)

(mg/L)	TDS [1]	Na^+	K^+	Ca^{2+}	Mg^{2+}	Cl^-	HCO_3^-
Mean	75341	30679	548	4532	851	43542	1130
Median	37099	25400	23	740	197	11000	412

1: Total dissolved solids.

Table 2—Testing conditions for two water chemistry scenarios

Scenarios	**High bicarbonate, low mineral cations**	**Low bicarbonate, high mineral cations**
Temperature / °C	50 - 70	70

P_{CO_2} / psia	35	3.5
[HCO_3^-] / (mg/L)	1000 - 3000	60 - 300
[Ca^{2+}] / (mg/L)	0 - 500	3000
[Mg^{2+}] / (mg/L)	0 - 600	500
pH	5.6 - 6.2	5.4 - 6.1
Solution Calcite SI	-0.4 to +0.5	-1.0 to +0.4
Specimen steel type	Mild steel, stainless steel	Mild steel, stainless steel

Results and Discussion

Corrosion Induced Scale Formation on Mild Steel

Firstly, a series of baseline tests without magnesium in the solution were conducted. The morphology of mild steel surface after 1 day testing is shown in **Fig. 2**. All tests showed a full coverage of scale on the steel surface. The corresponding phase identification of measured XRD patterns is shown in **Fig. 3**. It is worth noting that when calcium was present in the water, calcite formed on the mild steel surface even when the solution saturation index was slightly negative. At such a small saturation index, calcite formation would be usually deemed unlikely. Besides calcite, siderite ($FeCO_3$) formation is also detected. This indicates that calcite formation on the mild steel surface is different from that in the bulk solution, and siderite formed due to corrosion likely contributes to the calcite formation.

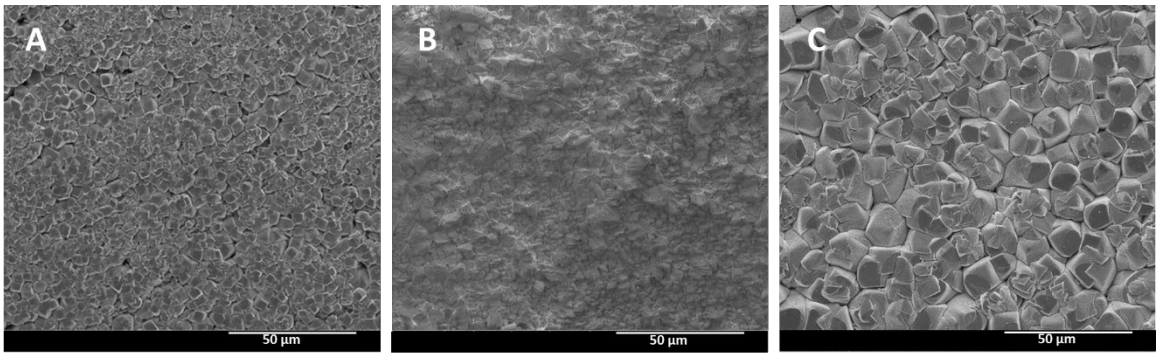

Fig. 2—Morphology of mild steel specimens after 1 day testing. 70 °C, 35 psia CO_2, pH: 6.2, 0.5 m (molality) NaCl, 3000 mg/L [HCO_3^-]. A: no calcium, B: 200 mg/L [Ca^{2+}] (calculated calcite SI = 0.4), C: 30 mg/L [Ca^{2+}] (calculated calcite SI = -0.4).

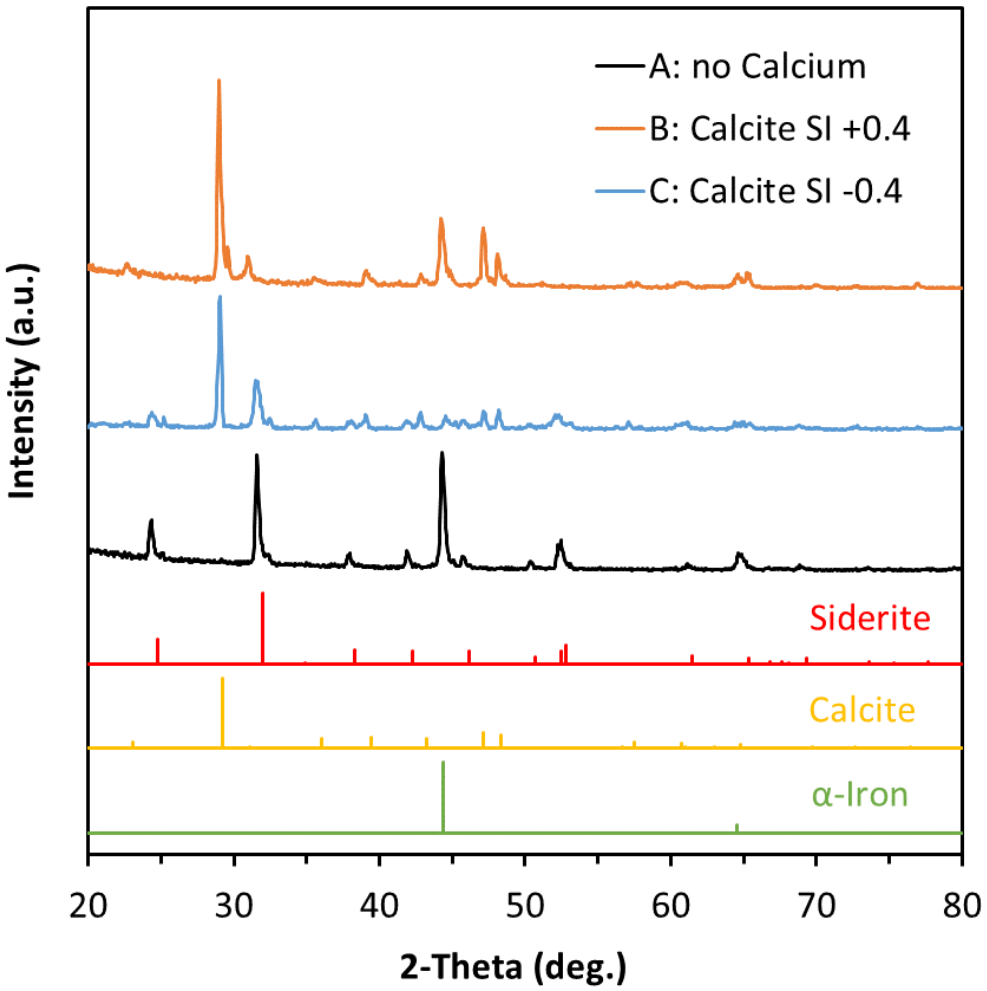

Fig. 3—XRD patterns of mild steel specimens after 1 day testing (as also seen in Fig. 2). A: no calcium, B: 200 mg/L [Ca^{2+}] (calculated calcite SI = 0.4), C: 30 mg/L [Ca^{2+}] (calculated calcite SI = -0.4).

In a following set of tests, magnesium ion with different ratios to calcium ion was added in the solution. Furthermore, both the high bicarbonate and low bicarbonate scenarios were investigated. The mild steel surface features after testing were examined by SEM, as shown in **Fig. 4**. For all testing conditions, a continuous rhombohedral scale layer was observed on the mild steel surface. Subsequent XRD measurements revealed some interesting results (shown in **Fig. 5**). For the high

bicarbonate scenario, a multi-cation carbonate, Ankerite (as $Ca(Fe_{0.73}\ Mg_{0.27})(CO_3)_2$) (Ross and Reeder 1992), was identified with various magnesium and calcium concentrations and ratios. On the contrary, only single cation carbonate formation, such as calcite or siderite, was found in the baseline tests shown earlier. Furthermore, it also differed from some studies in the open literature using ambient pressure glass cell, where siderite or dual-cation solid solution $Fe_xCa_{1-x}CO_3$ were often reported (Barker et al. 2018). This result demonstrates that the corrosion-induced scales can be complicated in different field water compositions. The formation of ankerite can be due to its relatively lower solubility, compared to conventional carbonate scales such as siderite. However, scarce literature on the topic of ankerite or other multi-cation carbonate solubility can be found (Railsback 1999), which warrants more studies in the future. For the low bicarbonate scenario, calcite was the only carbonate scale identified on the mild steel within 1 day. It is also noticeable that the bulk calcite SI was only 0.4, which is not deemed a high calcite formation driving force. This indicates that the corrosion process of mild steel, or the formation of the first corrosion induced scale layer, facilitated surface calcite deposition.

During the experiments, ferrous ion concentration from the testing cell effluent was monitored using a UV-vis spectrophotometer. The concentration was then used to calculate the instantaneous uniform corrosion rate of mild steel. The result is shown in Figure 6. Regardless, if it is ankerite or calcite scale formation, they both significantly reduced the mild steel corrosion rate within a day.

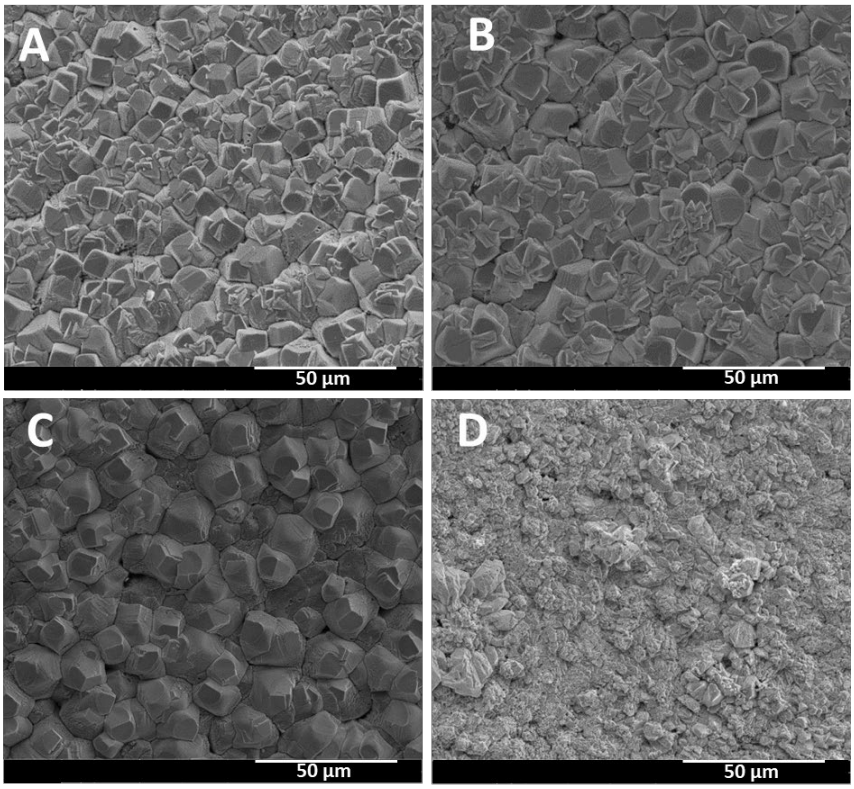

Fig. 4—Morphology of mild steel specimens after 1 day testing. 70 °C, pH: 6.1, 1.0 m NaCl.

A: 200 mg/L [Ca^{2+}] (calcite SI = 0.3), 67 mg/L [Mg^{2+}], 3000 mg/L [HCO_3^-], 35 psia CO_2.

B: 200 mg/L [Ca^{2+}] (calcite SI = 0.3), 600 mg/L [Mg^{2+}], 3000 mg/L [HCO_3^-], 35 psia CO_2.

C: 40 mg/L [Ca^{2+}] (calcite SI = -0.4), 120 mg/L [Mg^{2+}], 3000 mg/L [HCO_3^-], 35 psia CO_2.

D: 3000 mg/L [Ca^{2+}] (calcite SI = 0.4), 500 mg/L [Mg^{2+}], 300 mg/L [HCO_3^-], 3.5 psia CO_2.

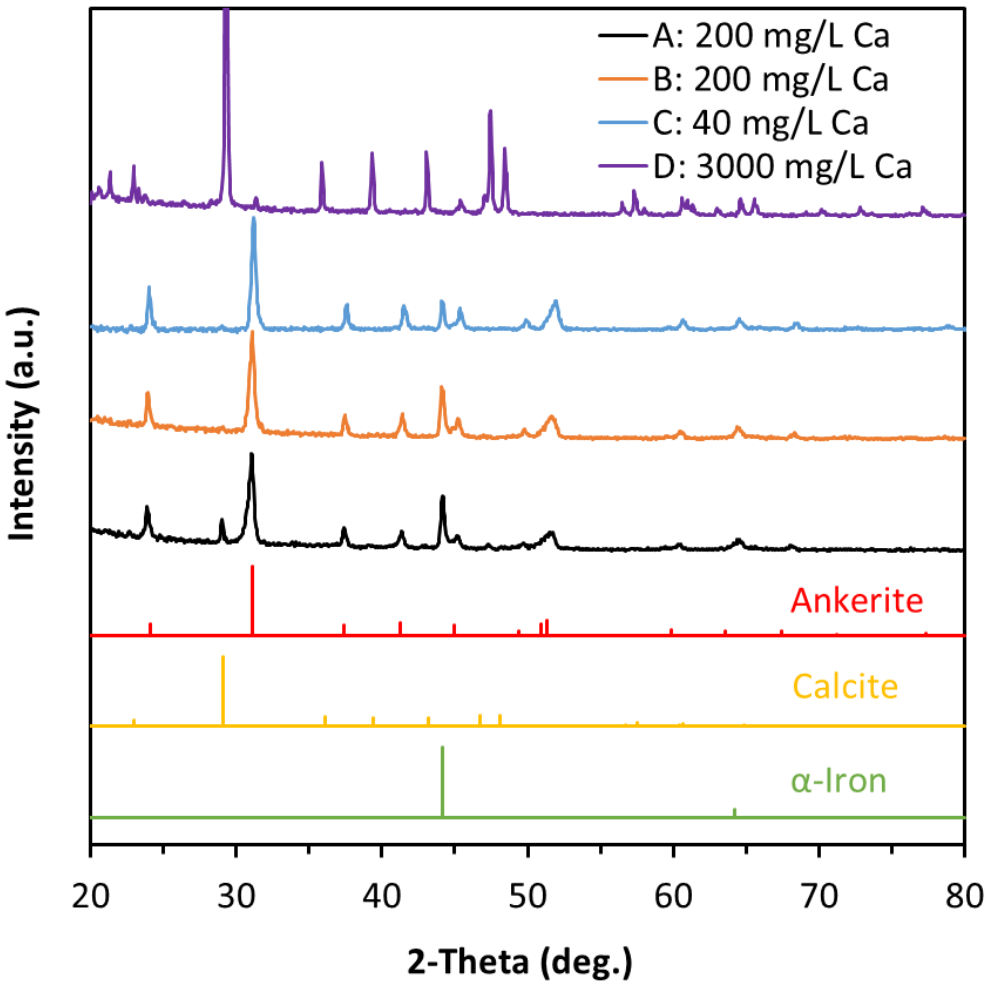

Fig. 5—XRD patterns of mild steel specimens after 1 day testing (morphology also see in Fig. 4). 70 °C, pH: 6.1, 1.0 m NaCl.

A: 200 mg/L [Ca^{2+}] (calcite SI = 0.3), 67 mg/L [Mg^{2+}], 3000 mg/L [HCO_3^-], 35 psia CO_2.

B: 200 mg/L [Ca^{2+}] (calcite SI = 0.3), 600 mg/L [Mg^{2+}], 3000 mg/L [HCO_3^-], 35 psia CO_2.

C: 40 mg/L [Ca^{2+}] (calcite SI = -0.4), 120 mg/L [Mg^{2+}], 3000 mg/L [HCO_3^-], 35 psia CO_2.

D: 3000 mg/L [Ca^{2+}] (calcite SI = 0.4), 500 mg/L [Mg^{2+}], 300 mg/L [HCO_3^-], 3.5 psia CO_2.

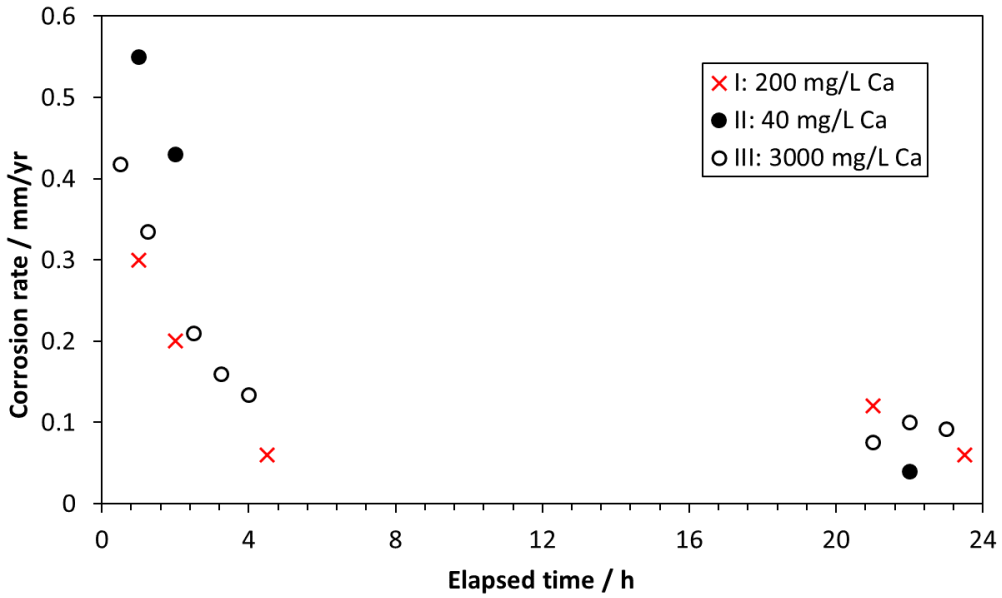

Fig. 6—Instantaneous corrosion rates of mild steel specimens during testing. 70 °C, pH: 6.1, 1.0 m NaCl.

I: 200 mg/L [Ca^{2+}] (calcite SI = 0.3), 67 mg/L [Mg^{2+}], 3000 mg/L [HCO_3^-], 35 psia CO_2.

II: 40 mg/L [Ca^{2+}] (calcite SI = -0.4), 120 mg/L [Mg^{2+}], 3000 mg/L [HCO_3^-], 35 psia CO_2.

III: 3000 mg/L [Ca^{2+}] (calcite SI = 0.4), 500 mg/L [Mg^{2+}], 300 mg/L [HCO_3^-], 3.5 psia CO_2.

As the corrosion rate decreases over time, one would expect a slower growth of ankerite because of limited amount of ferrous ion available on the steel surface. The following question was raised as to whether calcite or other metal carbonate scales can continue growing on top of the ankerite layer. Subsequently, a set of testing to understand the time effect was conducted. **Fig. 7** (A) and (B) show the post-test specimen morphology with 1-day and 2-day testing durations, respectively. A continuous scale layer formed on the steel for both tests. The backscattered SEM images show that a scale of about 10 μm thick formed on the 1-day test steel surface (shown in **Fig. 7** (C)). On

the other hand, two distinctive sub-layers (about 9 μm thick each) can be clearly seen on the 2-day test steel surface. EDS line scans for both tests clearly show the elemental profile changes across the two scale sublayers (**Fig. 7** (E) and (F)), which indicates the formation of metal carbonates. A noticeable increase of calcium from the inner to outer scale layer for both tests suggests a transition from iron carbonate to calcium carbonate scale toward the bulk solution.

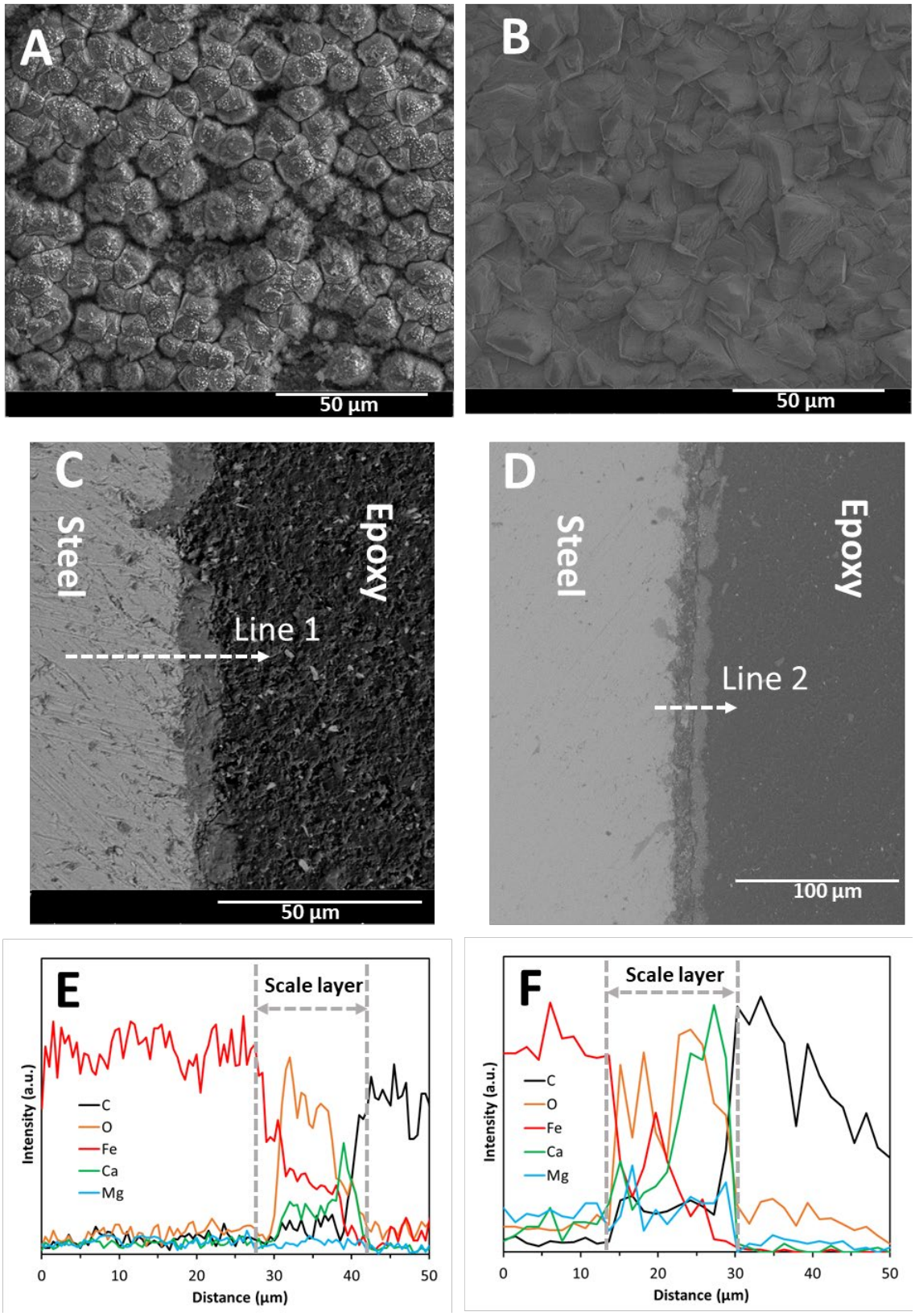
A
50 µm
B
50 µm
C
Steel
Epoxy
Line 1
50 µm
D
Steel
Epoxy
Line 2
100 µm
E
Scale layer
Intensity (a.u.)
C
O
Fe
Ca
Mg
0
10
20
30
40
50
Distance (µm)
F
Scale layer
Intensity (a.u.)
C
O
Fe
Ca
Mg
0
10
20
30
40
50
Distance (µm)

Fig.7—SEM-EDS analysis of mild steel specimens after testing. 70 °C, pH: 6.1, 1.0 m NaCl, 200 mg/L [Ca^{2+}] (calcite SI = 0.3), 67 mg/L [Mg^{2+}], 3000 mg/L [HCO_3^-], 35 psia CO_2.

A: top view, 1 day; B: top view, 2 days; C: cross-sectional view, 1 day; D: cross-sectional view, 2days; E: EDS scan of Line 1 (shown in C); F: EDS scan of Line 2 (shown in D).

XRD measurements on the samples from both tests were conducted to identify mineral phases on the steel surface, as shown in **Fig. 8**. Ankerite and calcite were found in both tests. Further reference intensity ratio (RIR) calculations revealed that the ankerite/calcite ratio changes from 1.3 to 0.04 for the 1-day and 2-day test, respectively. Combing with the information from **Fig. 2** and **Fig. 7** earlier, we believe that a two-layer scale structure is likely in this study. First, an inner iron-containing carbonate layer forms on the steel surface (e.g., siderite or ankerite). As the inner layer grows, corrosion slows down, and a transition to an outer calcite layer formation begins. Eventually, calcite continues to grow from the bulk solution, which then makes the system a classic calcite scaling problem. It is noted that the calcite deposition apparently is facilitated by the inner iron-containing scale, as the bulk calcite SI is small (up to 0.4) for the test results shown, which was deemed low scaling risk from the previous studies (Dai et al. 2021).

The morphology of stainless steel specimens is shown in **Fig. 9** to compare with the mild steel scale formation under the same testing conditions. No scale formed on the stainless steel specimens when mild steel specimens formed a continuous scale layer. In summary, we showed in this study that mild steel corrosion scale is crucial for further carbonate scale formation (i.e., calcite).

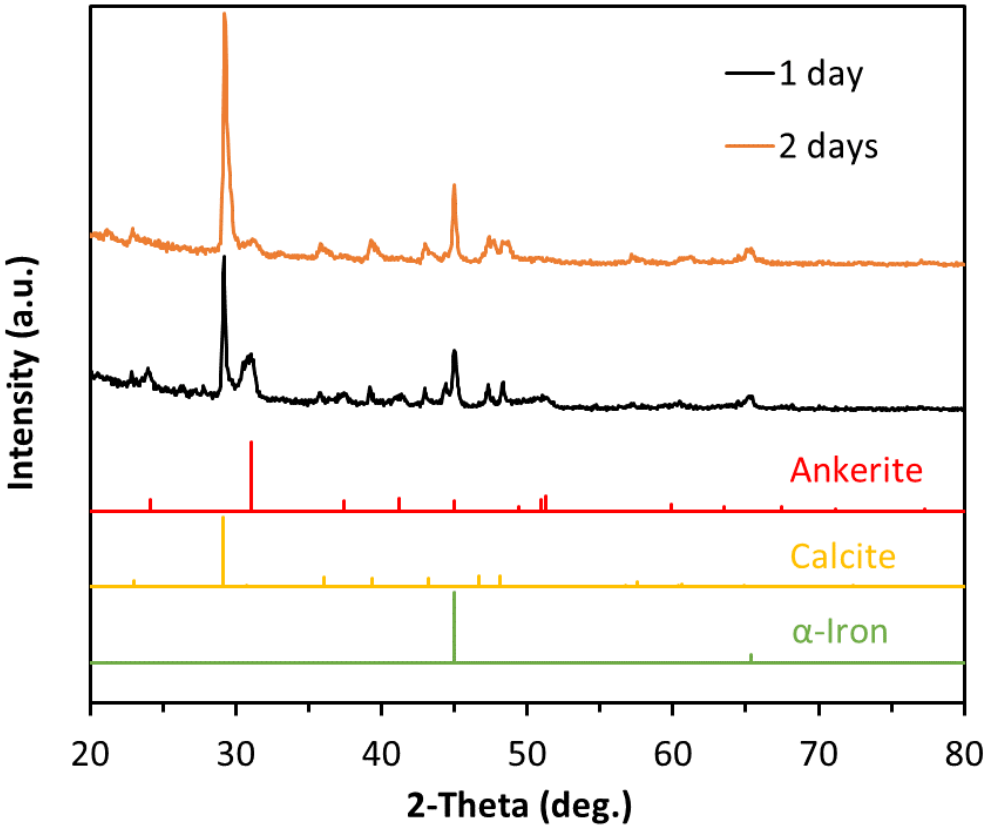

Fig. 8—XRD patterns of mild steel specimens after testing (as also seen in Fig. 7). 70 °C, pH: 6.1, 1.0 m NaCl, 200 mg/L [Ca^{2+}] (calcite SI = 0.3), 67 mg/L [Mg^{2+}], 3000 mg/L [HCO_3^-], 35 psia CO_2.

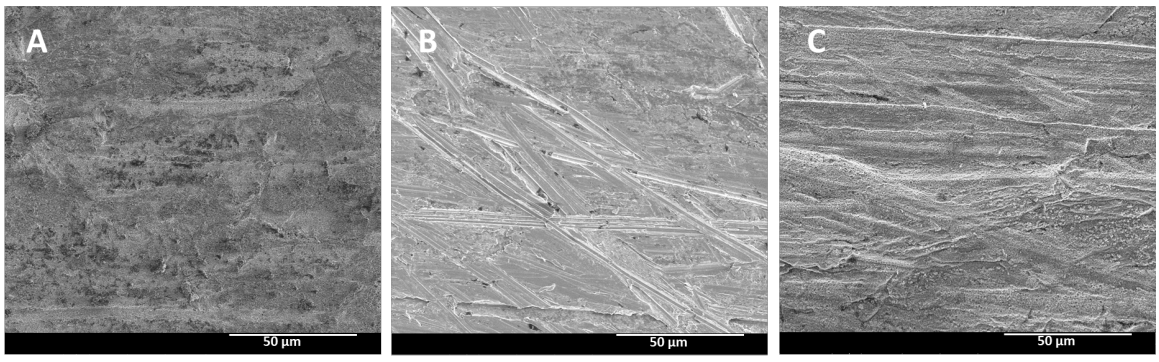

Fig. 9—Morphology of stainless steel specimens after testing. 70 °C, pH: 6.1, 1.0 m NaCl.

A: 3000 mg/L [Ca^{2+}] (calcite SI = 0.4), 500 mg/L [Mg^{2+}], 300 mg/L [HCO_3^-], 3.5 psia CO_2,1 day.

B: 200 mg/L [Ca^{2+}] (calcite SI = 0.3), 67 mg/L [Mg^{2+}], 3000 mg/L [HCO_3^-], 35 psia CO_2, 1 day.

C: 200 mg/L [Ca^{2+}] (calcite SI = 0.3), 67 mg/L [Mg^{2+}], 3000 mg/L [HCO_3^-], 35 psia CO_2, 2 days.

The sensitivities of the mild steel scale formation on pH and temperature were conducted. **Fig. 10** shows that a continuous scale layer formed at pH 5.6, 70 °C, and pH 6.1, 50 °C, respectively. Further XRD measurements on these specimens confirmed the presence of ankerite for both cases. This indicates ankerite formation is robust under the testing water chemistries at temperature range of 50 °C to 70 °C. Furthermore, ankerite formation has been previously reported at 200 °C and 20000 psia total pressure under simulated oilfield water chemistries (Tomson et al. 2015). Combining that with the findings from this study, it suggests that ankerite formation on mild steel can occur under a relatively large range of oil and gas production conditions.

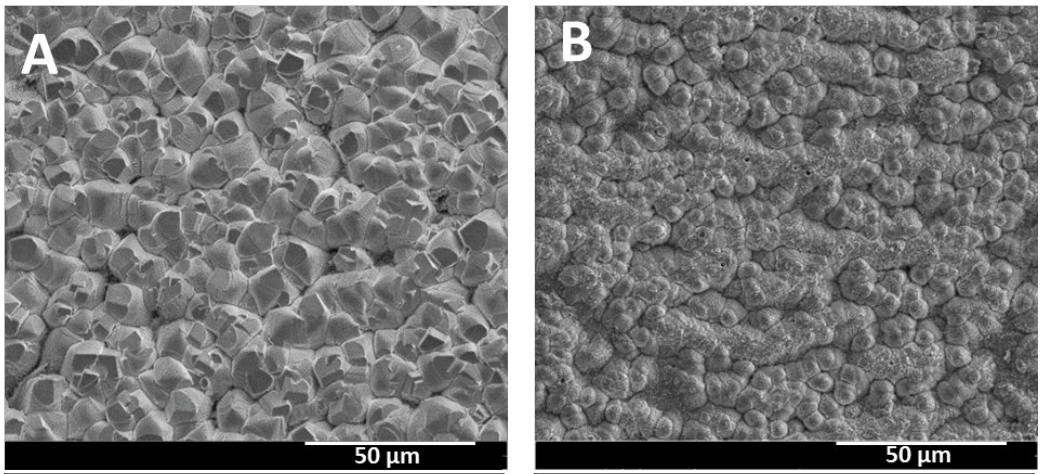

XRD phase identification
Ankerite
Iron

XRD phase identification
Ankerite
Calcite
Iron

Fig. 10—Morphology and phase identification on carbon steel specimens after testing.

A: 70 °C, pH: 5.6, 1.0 m NaCl, 340 mg/L [Ca^{2+}] (calcite SI = -0.4), 110 mg/L [Mg^{2+}], 1000 mg/L [HCO_3^-], 35 psia CO_2,1 day.

B: 50 °C, pH: 6.1, 1.0 m NaCl, 480 mg/L [Ca^{2+}] (calcite SI = 0.5), 160 mg/L [Mg^{2+}], 3000 mg/L [HCO_3^-], 35 psia CO_2, 2 days.

Inhibition of Corrosion Induced Scale on Mild Steel

Earlier we reported a two-layer scale formation on mild steel surface with an ankerite inner layer and calcite outer layer. The following question was raised as to whether this new scale structure would affect the performance of commonly used scale inhibitors. Therefore, a widely used calcite inhibitor, DTPMP (diethylenetriamine penta (methylenephosphonic acid)) was evaluated under both high and low bicarbonate scenarios described in **Table 2**. During a test, DTPMP was added to the anion stock solution and then injected into the testing cell continuously with other stock solutions. A starting dosage of 0.1 mg/L in the testing cell was used based on the minimum inhibitor concentration for calcite under the testing conditions calculated by the SSP software.

The post-test surface morphology of mild steel specimen for the low bicarbonate scenario is shown in Figure 11. Two distinctive zones were found on the steel surface. While the majority of surface appears to be scale free (**Fig. 11**A), mineral crystals are found in some isolated areas (**Fig. 11**B). It is noted that Ca, Mg, Fe, C, and O are found on the crystals when examined by SEM-EDS area scan, which may indicate formation of ankerite. However, only calcite was identified by XRD analysis, which may need further research in the future.

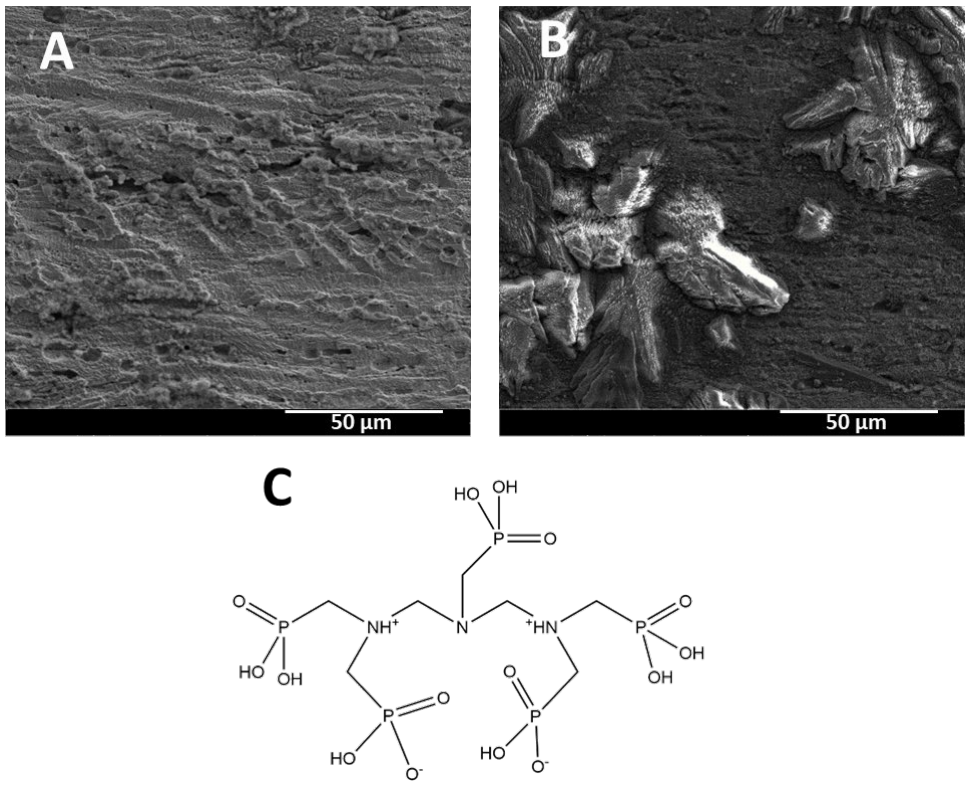

Fig.11—Morphology of carbon steel specimens after testing. 70 °C, pH: 6.1, 3.5 psia CO_2, 1.0 m NaCl, 3000 mg/L [Ca^{2+}] (calcite SI = 0.4), 500 mg/L [Mg^{2+}], 300 mg/L [HCO_3^-], 1 day, 0.1 mg/L DTPMP. A: the majority of steel surface features, B: the minority of steel surface features, C: DTPMP structure.

For the high bicarbonate scenario, two tests of identical testing conditions were conducted with 1-day and 2-day testing durations, respectively. **Fig. 12** shows both the top view and cross-sectional view SEM images after testing. Unlike the low bicarbonate results, a continuous scale layer can be seen for both tests. Further XRD measurements confirmed the presence of ankerite, as shown in **Fig. 13**. It appears that ankerite formation was not hindered in the presence of 0.1 mg/L DTPMP. However, no significant scale thickness growth between the 1-day and 2-day tests was observed from the cross-sectional images. On the contrary, calcite growth on ankerite in a 2-

day test was observed earlier under the same testing conditions without DTPMP (**Fig. 7**). This suggests that 0.1 mg/L DTPMP effectively inhibited calcite growth. It is also noted that calcite was identified on the 2-day test XRD result in addition to ankerite, even without significant scale thickness growth (**Fig. 13**). The mechanism is unclear at this moment, which warrants further research.

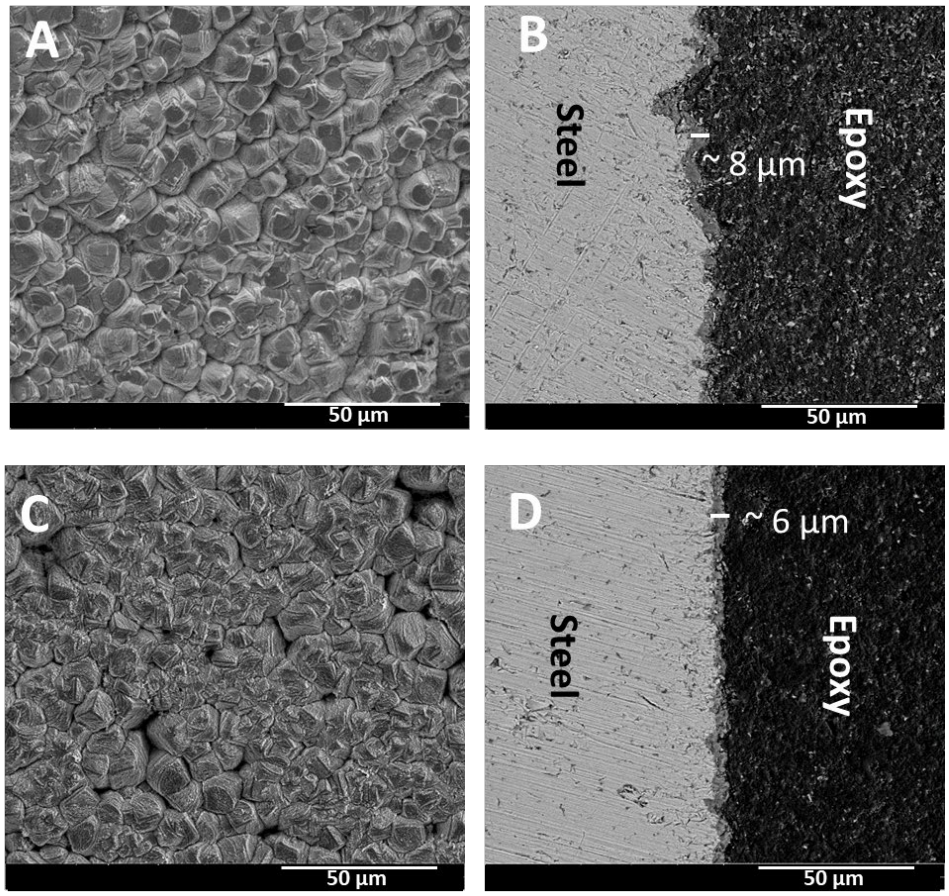

Fig. 12—SEM images of mild steel specimens after testing. 70 °C, pH: 6.1, 1.0 m NaCl, 200 mg/L [Ca^{2+}] (calcite SI = 0.3), 67 mg/L [Mg^{2+}], 3000 mg/L [HCO_3^-], 35 psia CO_2, 0.1 mg/L DTPMP. A: top view, 1 day; B: cross-sectional view, 1 day; C: top view, 2 days; D: cross-sectional view, 2days.

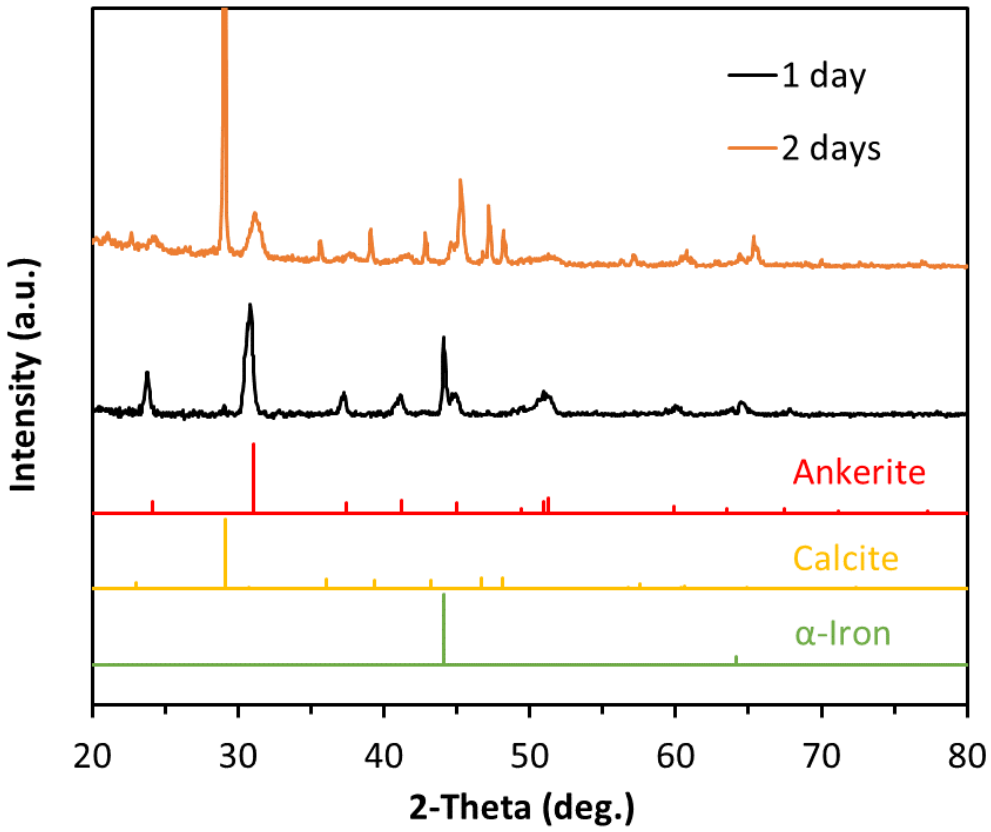

Fig. 13—XRD patterns of mild steel specimens after testing (as also seen in Fig. 12). 70 °C, pH: 6.1, 1.0 m NaCl, 200 mg/L [Ca^{2+}] (calcite SI = 0.3), 67 mg/L [Mg^{2+}], 3000 mg/L [HCO_3^-], 35 psia CO_2, 0.1 mg/L DTPMP.

To examine if DTPMP can inhibit formation of iron-containing carbonates such as siderite or ankerite, additional tests using higher dosages were conducted. **Fig. 14** shows the post-test mild steel surface features with 5.0 mg/L DTPMP in the water chemistry. No scale formed on the steel surface for both tests, suggesting that using a higher dosage of DTPMP is effective on ankerite inhibition.

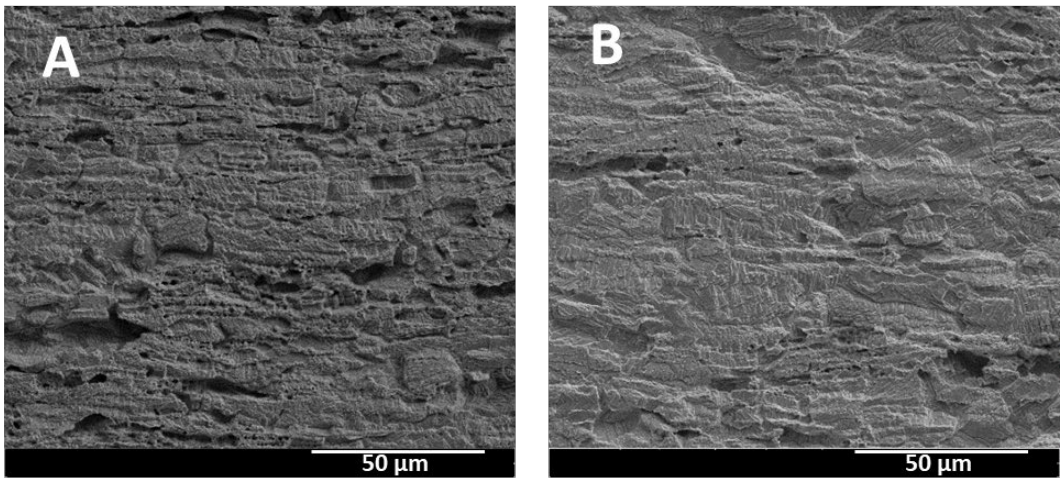

Fig. 14—SEM images of mild steel specimens after testing. 70 °C, pH: 6.1, 1.0 m NaCl, 200 mg/L [Ca^{2+}] (calcite SI = 0.3), 3000 mg/L [HCO_3^-], 35 psia CO_2, 1 day, 5.0 mg/L DTPMP. A: no Mg^{2+}; B: 67 mg/L [Mg^{2+}].

By far, we found that 0.1 mg/L DTPMP inhibited calcite formation on mild steel at a low bicarbonate water chemistry. However, the same dosage at a high bicarbonate water chemistry prevented calcite growth, but ankerite can still form on the steel surface. Furthermore, if a higher dosage of 5.0 mg/L DTPMP is used, the inhibitor can prevent any mineral carbonate formation on the mild steel surface.

In addition to the scaling study, the corrosion rates in the presence of scale inhibitor were also monitored, as shown in **Fig. 15**. It is noted that the effective carbonate scale inhibition with DTPMP in certain conditions (as shown in **Fig. 11** and **Fig. 14**) may also result in high corrosion rates of mild steel through the tests. On the other hand, continuous scale formation on the steel surface, such as calcite or ankerite, provides significant corrosion protection to the mild steel.

Therefore, corrosion and scale control should be considered holistically from field equipment integrity management point of view.

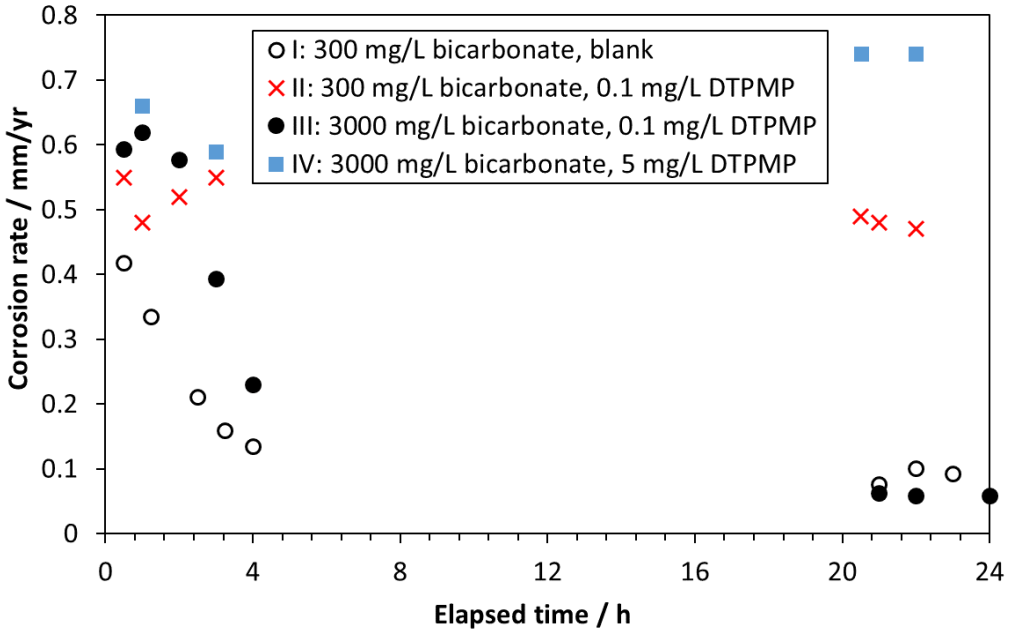

Fig. 15—Instantaneous corrosion rates of mild steel specimens during testing. 70 °C, pH: 6.1, 1.0 m NaCl.

I: 300 mg/L [HCO_3^-], no DTPMP, 3000 mg/L [Ca^{2+}] (calcite SI = 0.4), 500 mg/L [Mg^{2+}], 3.5 psia CO_2.

II: 300 mg/L [HCO_3^-], 0.1 mg/L DTPMP, 3000 mg/L [Ca^{2+}] (calcite SI = 0.4), 500 mg/L [Mg^{2+}], 3.5 psia CO_2.

III: 3000 mg/L [HCO_3^-], 0.1 mg/L DTPMP, 200 mg/L [Ca^{2+}] (calcite SI = 0.3), 67 mg/L [Mg^{2+}], 35 psia CO_2.

IV: 3000 mg/L [HCO_3^-], 5.0 mg/L DTPMP, 200 mg/L [Ca^{2+}] (calcite SI = 0.3), 67 mg/L [Mg^{2+}], 35 psia CO_2.

Discussion

The present results clearly demonstrate that a direct and complicated interaction between steel corrosion and mineral scaling exists. While both corrosion and scaling are common engineering issues for field operations, they normally are tended by different technical groups, e.g., materials integrity vs. flow assurance teams. Because of that, attention to the interaction between them is often omitted.

Carbonate scales like calcite and magnesite are common topics for scaling studies. However, water chemistry effect, including calcium, magnesium, and other cations found in produced water, is seldom considered in steel corrosion studies. These ions are often treated as additional salinity (ionic strength) effect in corrosion studies, and the predominant CO_2 corrosion product reported in the literature is still $FeCO_3$. The present results show that a predominant CO_2 corrosion product is actually ankerite under simulated produced water conditions, and the formed ankerite layer is also corrosion protective. One of the main challenges in CO_2 corrosion modeling is to predict the formation and protectiveness of corrosion product layer. The present research shows that complex carbonate corrosion product layer formation can take part in this challenge. It is not unusual to see a few thousand mg/L of calcium in produced water environments. There is certainly a possibility that a water chemistry has a large formation tendency for ankerite even if that for siderite is low.

On the other hand, for scaling researches, effect of corrosion on mineral scaling is often simulated through bulk water chemistry testing methods by adding ferrous ions, such as static bottle test and laser nucleation detection method (Zhang et al. 2019). Few studies focus on the interface between the steel and water environment, where the scale deposition occurs during production. The present results show that the ankerite corrosion product layer has a positive "anchoring" effect for further calcite deposition from the bulk solution, even when the bulk calcite

SI is low. This implies that corrosion product layer can promote calcite scaling issue which could otherwise get unnoticed using current knowledge on scaling prediction. This could bring scaling risk of deferring production operations.

In the present study, we find a significant impact of a complex carbonate corrosion product layer, ankerite, on both corrosion and scaling. Clearly further work is needed because ankerite was given little attention in the past for neither corrosion nor scale studies. For example, understanding on ankerite thermodynamics is limited, such as its solubility product constant, etc. The new research efforts will be crucial for accurate field corrosivity assessment and scaling prediction, as well as development of effective corrosion and scale control strategies.

Conclusions

In this study, we have reported complex metal carbonate formation, such as ankerite, on the mild steel surface under simulated oilfield environments due to corrosion.

We have also revealed that the iron-containing carbonate scale (e.g., ankerite and siderite) is crucial for promoting calcite deposition from the bulk water chemistry, even when the calcite SI is small that previously was deemed low scaling risk.

The mild steel corrosion induced scale exhibits a two-layer structure in this study. The inner layer is an iron-containing carbonate scale due to corrosion process such as ankerite or siderite, while the outer layer is calcite deposition from the bulk environment.

Finally, we have demonstrated that a conventional phosphonate calcite inhibitor (DTPMP) is still effective on calcite, siderite and ankerite inhibition on the mild steel surface at a proper concentration. However, such scale inhibition can lead to higher corrosion rates due to the absence

of the protective scale layer. Therefore, the control of mild steel sweet corrosion and the control of surface scale formation need to be considered simultaneously.

Acknowledgments

This work was financially supported by Brine Chemistry Consortium companies of Rice University, including Aegis, Baker Hughes, Chemstream, Chevron, Coastal Chemical, ConocoPhillips, Equinor, Flotek Industries, Halliburton, Hess, Imperative Chemicals, Irkutsk, Italmatch, JACAM, Kemira, Kinder Morgan, Kurita, Occidental, Petrobras, Pioneer, RSI, Saudi Aramco, Schlumberger, Shell, Smart Chemical, SNF, and Total. In addition, we acknowledge the support of the Shared Equipment Authority at Rice University for granting access to SEM, XRD and other analytical equipment.

References

Alsaiari, H. A., Kan, A., and Tomson, M. B. 2010. Effect of Calcium and Iron (II) Ions on the Precipitation of Calcium Carbonate and Ferrous Carbonate. *SPE J.*, **15**(2): 294–300. https://doi.org/10.2118/121553-PA

Amjad, Z., and Demadis, K. D. eds. 2015. *Mineral Scales and Deposits: Scientific and Technological Approaches*. Amsterdam, The Netherlands: Elsevier.

Barker, R., Burkle, D., Charpentier, T., Thompson, H., and Neville, A. 2018. A Review of Iron Carbonate ($FeCO_3$) Formation in the Oil and Gas Industry. *Corrosion Science*, **142**: 312–341. https://doi.org/10.1016/j.corsci.2018.07.021

Blondes, M.S., Gans, K.D., Engle, M.A., Kharaka, Y.K., Reidy, M.E., Saraswathula, V., Thordsen, J.J., Rowan, E.L., and Morrissey, E.A. 2018. U.S. Geological Survey National Produced Waters Geochemical Database, ver. 2.3. U.S. Geological Survey. https://doi.org/10.5066/F7J964W8

Bukuaghangin, O., Sanni, O., Kapur, N., Huggan, M., Neville, A., and Charpentier, T. 2016. Kinetics Study of Barium Sulphate Surface Scaling and Inhibition with a Once-through Flow

System. *J. Pet. Sci. Eng.*, **147**: 699–706. https://doi.org/10.1016/j.petrol.2016.09.035

Cavenati, S., Grande, C. A., and Rodrigues, A. E. 2006. Removal of Carbon Dioxide from Natural Gas by Vacuum Pressure Swing Adsorption. *Energy and Fuels*, **20**(6): 2648–2659. https://doi.org/10.1021/ef060119e

Dai, Z., Lu, Y. T., Kan, A., Leschied, C., Zhao, Y., Dai, C., Wang, X., Paudyal, S., Ko, S., and Tomson, M. 2021. A Mechanistic Software Platform for Mineral Surface Deposition and Inhibition Prediction under Different Flow Conditions. *Desalination*, **509**: 115071. https://doi.org/10.1016/j.desal.2021.115071

Danesh, A. 1998. *PVT and Phase Behaviour of Petroleum Reservoir Fluids*. Amsterdam, The Netherlands: Elsevier.

Ding, C., Gao, K. W., and Chen, C. F. 2009. Effect of Ca^{2+} on CO_2 Corrosion Properties of X65 Pipeline Steel. *International Journal of Minerals, Metallurgy and Materials*, **16**: 661–666. https://doi.org/10.1016/S1674-4799(10)60009-X

Fogler, H. S. 2019. *Elements of Chemical Reaction Engineering*, fifth edition. Boston, MA: Prentice Hall.

Greenberg, J., and Tomson, M. 1992. Precipitation and Dissolution Kinetics and Equilibria of Aqueous Ferrous Carbonate vs Temperature. *Applied Geochemistry*, **7**(2): 185–190. https://doi.org/10.1016/0883-2927(92)90036-3

Harouaka, K., Lu, Y. T., Ruan, G., Sriyarathne, H. D., Li, W., Deng, G., Zhao, Y., Wang, X., Kan, A. T., and Tomson, M. 2018. The Effect of Surface Material on the Mechanics of Calcium Carbonate Scale Deposition. Paper presented at the SPE International Oilfield Scale Conference and Exhibition, Aberdeen, Scotland, UK, June 2018. SPE-190700-MS. https://doi.org/10.2118/190700-MS

Hubbard, C. R., and Snyder, R. L. 1988. RIR — Measurement and Use in Quantitative XRD. *Powder Diffraction*, **3**(2): 74–77. https://doi.org/10.1017/S0885715600013257

Ieamsupapong, S., Brown, B., Singer, M., and Nesic, S. 2017. Effect of Solution pH on Corrosion Product Layer Formation in a Controlled Water Chemistry System. Paper presented at the NACE International Corrosion Conference. Paper no. 9160.

Javaherdashti, R., Nwaoha, C., and Tan, H. eds. 2013. *Corrosion and Materials in the Oil and Gas Industries*. Boca Raton, FL:CRC Press.

Johnson, M. L., and Tomson, M. 1991. Ferrous Carbonate Precipitation Kinetics and Its Impact CO_2 Corrosion. Paper presented at the NACE International Corrosion Conference. Paper no. 268.

Joshi, G. R., Cooper, K., Zhong, X., Cook, A. B., Ahmad, E. A., Harrison, N. M., Engelberg, D. L., and Lindsay, R. 2018. Temporal Evolution of Sweet Oilfield Corrosion Scale: Phases, Morphologies, Habits, and Protection. *Corrosion Science*, **142**: 110–118. https://doi.org/10.1016/j.corsci.2018.07.009

Kahyarian, A., Achour, M., and Nesic, S. 2017. Mathematical Modeling of Uniform CO_2 Corrosion. In *Trends in Oil and Gas Corrosion Research and Technologies*. Cambridge, MA: Woodhead Publishing.

Kan, A. T., Dai, J. Z., Deng, G., Ruan, G., Li, W., Harouaka, K., Lu, Y. T., Wang, X., Zhao, Y., and Tomson, M. B. 2018. Recent Advances in Scale Prediction, Approach, and Limitations. Paper presented at the SPE International Oilfield Scale Conference and Exhibition, Aberdeen, Scotland, UK, June 2018. SPE-190754-MS. https://doi.org/10.2118/190754-MS

Kelland, M. A. 2014. *Production Chemicals for the Oil and Gas Industry*, second edition. Boca Raton, FL: CRC Press.

Li, W., Brown, B., Young, D., and Nesic, S. 2014. Investigation of Pseudo-Passivation of Mild Steel in CO_2 Corrosion. *Corrosion*, **70**(3): 294–302. https://doi.org/10.5006/0950

Li, W., Pots, B. F. M., Brown, B., Kee, K. E., and Nesic, S. 2016. A Direct Measurement of Wall Shear Stress in Multiphase Flow-Is It an Important Parameter in CO_2 Corrosion of Carbon Steel Pipelines? *Corrosion Science*, **110**: 35–45. https://doi.org/10.1016/j.corsci.2016.04.008

Li, W., Ruan, G., Bhandari, N., Wang, X., Liu, Y., Sriyarathne, H. D., Harouaka, K., Lu, Y. T., Deng, G., Zhao, Y., Kan, A. T., and Tomson, M. 2018. Development of Novel Iron Sulfide Scale Control Chemicals. Paper presented at the SPE International Oilfield Scale Conference and Exhibition, Aberdeen, Scotland, UK, June 2018. SPE-190755-MS. https://doi.org/10.2118/190755-MS

Li, W., Xiong, Y., Brown, B., Kee, K. E., and Nesic, S. 2015. Measurement of Wall Shear Stress in Multiphase Flow and Its Effect on Protective $FeCO_3$ Corrosion Product Layer Removal. Paper presented at the NACE International Corrosion Conference. Paper no. 5922.

Lu, A. Y. T., Harouaka, K., Paudyal, S., Ko, S., Dai, C., Gao, S., Deng, G., Zhao, Y., Wang, X., Mateen, S., Kan, A. T., and Tomson, M. 2020. Kinetics of Barium Sulfate Deposition and Crystallization Process in the Flowing Tube. *Industrial and Engineering Chemistry Research*, **59**(16): 7299–7309. https://doi.org/10.1021/acs.iecr.0c00112

Mansoori, H., Brown, B., Young, D., Nesic, S., and Singer, M. 2019. Effect of $Fe_xCa_yCO_3$ and $CaCO_3$ Scales on the CO_2 Corrosion of Mild Steel. *Corrosion*, **75**(12): 1434–1449. https://doi.org/10.5006/3290

Nesic, S. 2012. Effects of Multiphase Flow on Internal CO_2 Corrosion of Mild Steel Pipelines. *Energy and Fuels*, **26**(7): 4098–4111. https://doi.org/10.1021/ef3002795

Railsback, L. B. 1999. Patterns in the Compositions, Properties, and Geochemistry of Carbonate Minerals. *Carbonates and Evaporites*, **14**(1), 1–20. https://doi.org/10.1007/BF03176144

Ross, N. L., and Reeder, R. J. 1992. High-Pressure Structural Study of Dolomite and Ankerite. *American Mineralogist*, **77**(3–4): 412–421.

Tomson, R. C., Yan, C., Guraieb, P., and Tomson, M. B. 2015. Corrosion and Scale at Extreme Temperature and Pressure. RPSEA Phase 2 Final Technical Report, Tomson Technologies LLC, Houston, TX.

Zhang, P., Zhang Z., Liu Y., Kan, A. T., and Tomson, M. B. 2019. Investigation of the Impact of Ferrous Species on the Performance of Common Oilfield Scale Inhibitors for Mineral Scale Control. *Journal of Petroleum Science and Engineering*, **172**: 288–296. https://doi.org/10.1016/j.petrol.2018.09.069